College of Arts and Sciences

Mat. Res. Soc. Symp. Proc. Vol. 731 © 2002 Materials Research Society

Migration of Aluminum Atoms in the Transformation of γ– to θ–Alumina

Shu-Hui Cai[1,2] and Karl Sohlberg[2]
[1]Department of Physics, Xiamen University, Xiamen 361005, P.R.C.
[2]Department of Chemistry, Drexel University, Philadelphia, PA 19104, U.S.A.

ABSTRACT

γ– and θ–alumina are two metastable phases of aluminum oxide observed along the thermal dehydration sequence of boehmite before conversion to the final product α–alumina. The transformation from γ– to θ–alumina was studied by using $Al_{16}O_{24}$ cells. Motion of some Al atoms from their γ–alumina positions to new positions and no O motions result in an approximate structure that, upon relaxation by first-principles calculations, becomes the known θ–alumina structure. Total-energy calculations along the paths of the atomic motions have been used to map out transformation pathways. The model accurately predicts experimentally observed domain boundaries in θ–alumina and the γ– to θ–alumina conversion rate.

INTRODUCTION

Alumina, (nominally Al_2O_3) is an exceptionally significant structural and functional ceramic material that has stimulated many experimental and theoretical investigations [1–8]. The dehydration sequence of the alumina precursor boehmite (γ–AlOOH) upon thermal treatment,

$$\text{boehmite} \rightarrow \gamma \rightarrow \delta \rightarrow \theta \rightarrow \alpha$$

is particularly interesting since the transitional γ–alumina form is of such considerable industrial importance. The γ–alumina form finds particularly widespread use in catalysis, due in large part to its high porosity and surface area [3]. One serious problem is that at elevated temperatures (1000–1100°C), undoped γ–alumina transforms rapidly to α–alumina, accompanied by a catastrophic loss of porosity via sintering. Stabilization of γ–alumina, therefore, represents an important industrial and commercial problem. Clearly, an understanding of the mechanisms of the polymorphic transformations would be of great value in developing improved material preparation for control of sintering. In this work we study the phase transition of γ– to θ–alumina by first principles calculations. The picture provided here shows how aluminum cations are reordered to form θ–alumina from γ–alumina and the possible mechanism for such reordering.

COMPUTATION METHOD

The theoretical results were obtained based on density functional theory (DFT) [9] with the PW91 generalized gradient approximation (GGA) to the exchange-correlation energy [10], as described in the review by Payne et al. [11] and coded in the program CASTEP. The electron-ion interactions were described with ultrasoft pseudopotentials [12]. A plane wave basis was used to describe the electronic wavefunction with a cutoff energy of 380 eV. Test calculations indicated that a 380 eV cutoff energy was sufficient to obtain converged energy differences and structural properties for the investigated systems. Integrations over the Brillouin zone employed a grid of

k-points with a spacing of 0.1 /Å chosen according to the Monkhorst-Pack scheme [13]. Vibrational frequencies of Al atom were estimated in the harmonic approximation by diagonalizing the mass-weighted Cartesian force constant matrix applicable to the Al atom in question [14].

RESULTS

Although the structures of γ– and θ–alumina look rather different (cubic and monoclinic symmetry, respectively) [5,15], both have a face-centered-cubic (*fcc*) oxygen anion sublattice with aluminum cations occupying a portion of the available octahedral (O_h) and tetrahedral (T_d) interstices. Naturally, it is supposed that the phase transition of γ– to θ–alumina occurs by the migration of aluminum cations among the O_h and T_d sites available in oxygen anion sublattice, which does not change appreciably during transformation.

Comparison of the structures of γ– and θ–alumina reveals that the unit cells of γ– and θ–alumina can be redefined to similar shapes. We first define a new γ–alumina unit cell in terms of the basis vectors of its cubic cell $\boldsymbol{a}_\gamma$, $\boldsymbol{b}_\gamma$ and $\boldsymbol{c}_\gamma$, such that

$$\boldsymbol{a}_{\gamma N} = 1.5\boldsymbol{a}_\gamma + 0.5\boldsymbol{b}_\gamma \quad (1)$$

$$\boldsymbol{b}_{\gamma N} = -0.5\boldsymbol{b}_\gamma + 0.5\boldsymbol{c}_\gamma \quad (2)$$

$$\boldsymbol{c}_{\gamma N} = -0.5\boldsymbol{b}_\gamma - 0.5\boldsymbol{c}_\gamma, \quad (3)$$

where $\boldsymbol{a}_{\gamma N}$, $\boldsymbol{b}_{\gamma N}$ and $\boldsymbol{c}_{\gamma N}$ are the unit vectors of the redefined cell (cell γ_N, figure 1a). Next we enlarge the θ–alumina unit cell Al_8O_{12} to a cell containing $Al_{16}O_{24}$ (cell θ_N, figure 1b) using new unit vectors

$$\boldsymbol{a}_{\theta N} = \boldsymbol{a}_\theta - \boldsymbol{b}_\theta \quad (4)$$

$$\boldsymbol{b}_{\theta N} = 2\boldsymbol{b}_\theta \quad (5)$$

$$\boldsymbol{c}_{\theta N} = \boldsymbol{c}_\theta, \quad (6)$$

where $\boldsymbol{a}_\theta$, $\boldsymbol{b}_\theta$ and $\boldsymbol{c}_\theta$ are the basis vectors of θ–alumina, and $\boldsymbol{a}_{\theta N}$, $\boldsymbol{b}_{\theta N}$ and $\boldsymbol{c}_{\theta N}$ are the unit vectors of the supercell. The essential difference between γ_N and θ_N is only in the distribution of Al atoms in the interstices among the *fcc* oxygen sublattice. The striking similarity can be seen in figure 1.

There are two *direct* pathways that transform cell γ_N into a cell similar to θ_N. (Here "direct" implies that Al atoms move to adjacent unoccupied T_d or O_h sites). These two transformation paths give us two ways to construct a model θ–alumina cell from the redefined cell γ_N. Scheme **A**: Keep two 8a and six 16d aluminum atoms at their original sites (assume no vacancies in these sites), the remaining eight aluminum atoms move to two 16c and six 48f sites (yields model **A**). Scheme **B**: Keep two 16d aluminum atoms, all other aluminum atoms move to six 16c, two 8b and six 48f sites (yields model **B**). The resulting models are shown in figure 2. For easier comparison, two unit cells are shown. Disregarding the small distortion, models **A** and **B** are translationally equivalent, correlated by translation vector $\boldsymbol{R} = \boldsymbol{c}_{\gamma N}/2$. Models **A** and **B** can each be constructed in three equivalent ways, depending on different sets of 8a and 16d sites occupied. The three **A** (or **B**) variants can be approximately generated from one of them by translation vectors: $\boldsymbol{R} = \boldsymbol{a}_{\gamma N}/6 - \boldsymbol{b}_{\gamma N}/6 + \boldsymbol{c}_{\gamma N}/3$ and $\boldsymbol{R} = \boldsymbol{a}_{\gamma N}/3 + \boldsymbol{b}_{\gamma N}/6 + 2\boldsymbol{c}_{\gamma N}/3$. Exchanging $b_{\gamma N}$ and $c_{\gamma N}$ axes gives equivalent results. If the oxygen anions of γ–alumina are in ideal positions (μ = 0.375, but not 0.387 as we used in calculations) the constructed θ models can be further simplified to Al_8O_{12} with structure similar to θ–alumina reported experimentally.

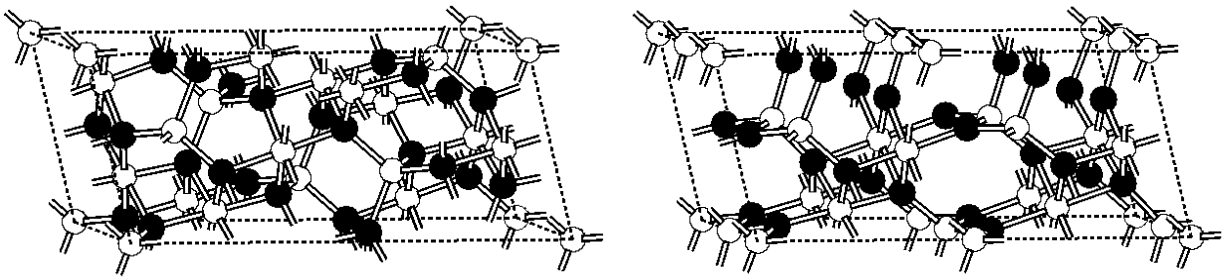

(a) (b)

Figure 1. (a) Defect-free cell γ_N; (b) cell θ_N with translation of origin (solid spheres: oxygen, empty sphere: aluminum). Note that the anion sublattices are identical.

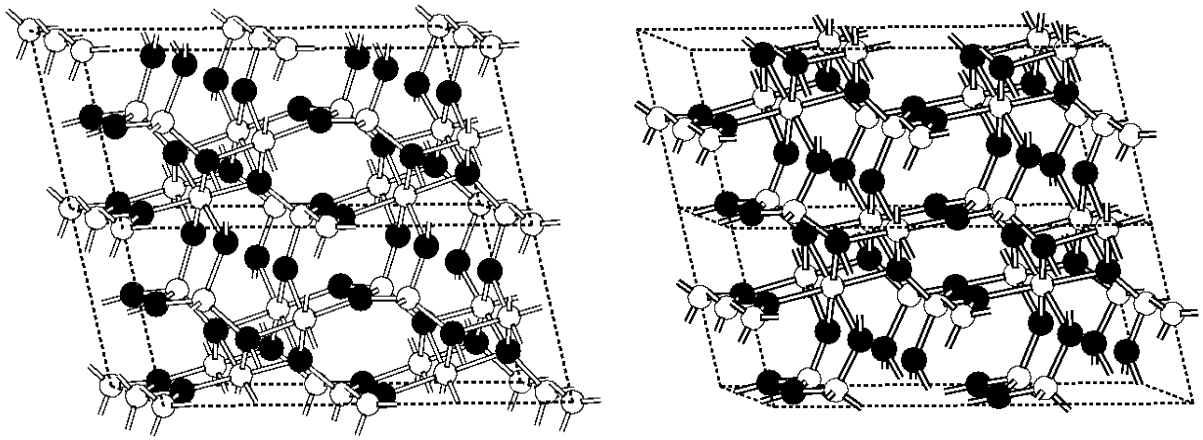

(a) (b)

Figure 2. Two θ models constructed from γ–alumina: (a) Model **A**; (b) Model **B** (solid spheres: oxygen, empty sphere: aluminum). **A** and **B** are translationally equivalent.

First principles total energy calculations and full geometry optimizations have been carried out on the two θ models and the experimental θ–alumina structure [15]. The geometric parameters and the related total energies are listed in table 1. Upon optimization, the two model structures and the experimental structure yield essentially identical structures. The cell parameters differ by less than 1%, and are consistent with earlier theoretical calculations [8,16]. The energy differences are within 0.002 eV/Al_2O_3. The symmetries of the optimized structures of the two models and the experimental θ–alumina structure are all $C2/m$ within the limits of accuracy of the calculations. Average Al–O bond lengths are also very similar. Taken collectively, these results indicate that the approximate and experimental θ–alumina optimize to the same structure within the margins of error of the model.

Based on the relationship of lattice axes between γ_N–alumina and γ–alumina, the orientation relationship between γ–alumina and θ models (no matter simplified or not) can be deduced to be $[010]_\theta \| [0\,\bar{1}\,1]_\gamma$ (or $[010]_\theta \| [0\,\bar{1}\,\bar{1}]_\gamma$ when $b_{\gamma N}$ and $c_{\gamma N}$ axes are exchanged) and $(100)_\theta \| (100)_\gamma$,

equivalent to the experimental results of $[010]_\theta \| [110]_\gamma$ and $(100)_\theta \| (001)_\gamma$ [6] according to lattice symmetry [6,17].

There are five possible paths for the migration of aluminum atoms directly to nearby interstitial sites of the oxygen anion sublattice of γ–alumina to form θ–alumina: (a) 8a to 16c; (b) 16d to 48f; (c) 8a to 48f; (d) 16d to 16c; (e) 16d to 8b (only for model **B**). Consider migration of one aluminum atom only. First principles calculations show that the energy differences between the structures before and after Al migration are all very large due to strong Al–Al repulsive interactions (Al–Al bonds) when no vacancies are around the destination. They decrease when the number of Al–Al bonds decreases. Therefore, it is easier for the migration of aluminum atoms to happen in the vicinity of vacancies. Our calculations show that the configuration with pure O_h vacancies widely separated is lowest in energy among configurations with pure O_h or T_d vacancies limited to the sites unoccupied in θ models. This is consistent with previous theoretical calculations [8]. Starting from this lowest energy configuration of γ_N, we moved Al atoms to their destinations one by one to determine the lowest energy intermediate states of model **A**. All structural parameters of intermediate states are optimized except lattice parameters. It is found that only six steps are necessary for the migration of eight aluminum atoms to transform γ_N to model **A**. The last two Al atoms relax to their destinations spontaneously following the migration of the sixth aluminum atom. On the basis of the migration sequence, we searched for the transition states for every step by successively fixing the position of the migrating atom and another atom far away from it and relaxing all other atoms. The energy variation with the aluminum migration is shown in figure 3.

The rate r at which a step takes place is determined by the frequency v with which reactants approach the top of the barrier, the population of the reactants f, and the probability that the reactants have sufficient energy to surmount the barrier $\rho(E > \Delta E)$, *i.e.*,

$$r = vf\rho(E > \Delta E), \tag{7}$$

where

$$\rho(E > \Delta E) = \frac{1}{kT}\int_{\Delta E}^{\infty} e^{-E/kT}\,dE\,. \tag{8}$$

Here k is the Boltzmann constant, and T is the Kelvin temperature.

Assuming that quasi-equilibria are set up among the species preceding the rate-controlling step, Boltzmann statistics were employed to estimate the population of the intermediate precursor to the rate-controlling step i,

$$f_i = \frac{e^{-E_i/kT}}{\sum_{l=1}^{i} e^{-E_l/kT}} \tag{9}$$

where E_l is the energy of the species l. Here $i = 4$.

Table 1. Comparison of structural parameters for models of θ–alumina (Distances in Å, angles in degree, energies in eV/Al_2O_3)

Species	a	b	c	α	β	γ	ΔE	Al_{Oh}-O	Al_{Td}-O
Exp. [15]	12.20	5.808	5.622	90	103.4	103.8	––	1.948	1.760
Exp. (opt) [15]	12.13	5.733	5.532	90.00	103.5	103.7	0	1.909	1.737
Model **A**	12.20	5.727	5.529	89.85	103.7	103.8	–0.002	1.911	1.738
Model **B**	12.22	5.719	5.529	89.90	103.6	103.8	0.0006	1.910	1.738

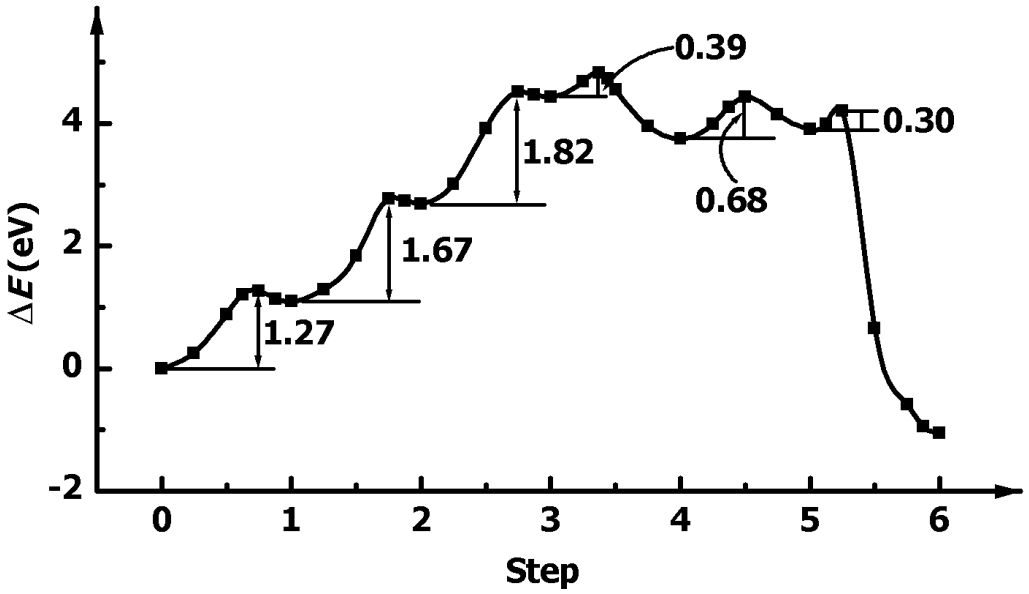

Figure 3. The energy profile along the reaction pathway

The calculated rate at 1300 K is 1.76×10^{-5} s^{-1}, which implies that about 11 hours are required for half of the reactants to surmount the barrier of step 4, in excellent agreement with the experimental conversion time.

The transformation path for γ– to θ–alumina by scheme **B** should be much slower than by model **A**: First of all, there are six more steps by scheme **B**, rendering it statistically less probably, and secondly, the Al atoms moving to 8b sites, (a step that only occurs in scheme **B**) encounter one more Al−Al repulsive interaction than those to 16c and 48f sites having the same number of adjacent vacancies, making scheme **B** energetically less favorable as well. Of course, due to randomness in the distribution of Al vacancies, numerous Al migration paths are possible, thus forming the variants of models **A** and **B** in different domains. This may be the reason for the formation of twins and interfaces in θ–alumina [17].

To account for the extension of a_γ by 3/2, Levin and coworkers believed that the transformation from γ– to θ–alumina must proceed through disordering of the γphase to a simple *fcc* structure with a_γ reduced by 2, and then reordering with a threefold increase of the lattice parameter (resulting in $a_\theta = 3/2a_\gamma$) [5]. For this disordering transition to occur, all the O_h (d and c) and T_d (a, b and f) cation sites should become equivalent. Our study shows that $3/2a_\gamma$ is easily explained by the θ models constructed from γ_N cell, although $a_{\gamma_N} = (5/2)^{1/2}a_\gamma$, a_θ can be simplified to $3/2a_\gamma$ by neglecting the small distortion of oxygen sublattice. It may be true that the lattice symmetry nominally becomes $Fm\bar{3}m$ during the $\gamma$to θ transformation process by scheme **B** owing to the large scale of rearrangement of Al sublattice and the involvement of 8b sites, but it seems unnecessary to satisfy such a restriction in the domain where the transformation takes the path of scheme **A** and 8b sites are not involved.

CONCLUSIONS

The transformation of γ– to θ–alumina has been studied by $Al_{16}O_{24}$ cells that have similar cell parameters. It is found that when some of the aluminum atoms in γ–alumina move to specific sites, a close approximation of θ–alumina is formed. The orientation relationship between γ–alumina and θ models agrees with experimental measurements. The approximate and experimental θ–alumina optimize to the same structure within the margins of error of the models. The aluminum migration is proposed to take place first in the vicinity of cation vacancies to reduce strong Al–Al interactions. Moving Al atoms one by one, the lowest-energy pathway for the transformation is mapped out. The computed conversion rate recovers the experimental transformation temperature with high accuracy. The formation of interfaces in θ–alumina can be explained by different aluminum migration paths in neighboring domains during γ– to θ–alumina transformation.

ACKNOWLEDGMENTS

This work was supported in part by the USDOE under contract number DE-FC02-01CH11085 and by an NSF GOALI Grant DMR-0111841 with Alcoa, Inc.

REFERENCES

1. H. Knözinger and P. Ratnasamy, *Catal. Rev.-Sci. Eng.* **17**, 31 (1978).
2. M. Che and C. O. Bennett, *Adv. Catal.* **36**, 55 (1989).
3. C. N. Satterfield, *Heterogeneous Catalysis in Practice*, (McGraw-Hill: New York, 1980), section 4.5.
4. B. C. Gate, *Chem. Rev.* **95**, 511 (1995).
5. K. Wefers and C. Misra, *Oxides and Hydroxides of Aluminum* (Alcoa, 1987).
6. I. Levin and D. Brandon, *J. Am. Ceram. Soc.* **81**, 1995 (1998) and references therein.
7. K. Sohlberg, S. J. Pennycook and S. T. Pantelides, *Chem. Eng. Comm.* **181**, 107 (2000).
8. C. Wolverton and K. C. Hass, *Phys. Rev. B* **63**, 024102 (2001) and references therein.
9. W. Kohn and L. J. Sham, *Phys. Rev.* **140A**, 1133 (1965).
10. J. P. Perdew, *Phys. Rev. B* **33**, 8822 (1986).
11. M. C. Payne, M. P. Teter, D. C. Allan, T. A. Arias and J. D. Joannopoulos, *Rev. Mod. Phys.* **64**, 1045 (1992).
12. D. Vanderbilt, *Phys. Rev. B* **41**, 7892 (1990).
13. H. J. Monkhorst and J. D. Pack, *Phys. Rev. B* **13**, 5188 (1976).
14. K. Sohlberg, S. J. Pennycook and S. T. Pantelides, *Recent Research Developments in Physical Chemistry*, **4(part I**), 71 (2000).
15. R-S. Zhou and R. L. Snyder, *Acta Cryst.* **B47**, 617 (1991) and references therein.
16. A. P. Borosy, B. Silvi, and M. Allavena, *J. Phys. Chem.* **98**, 13189 (1994).
17. I. Levin, L. A. Bendersky, D. G. Brandon and M. Rühle, *Acta Mater*. **45**, 3659 (1997).